Molecular dynamics simulation study on the isomerization reaction in a solvent with slow structural relaxation

Tsuyoshi Yamaguchi*
Graduate School of Engineering, Nagoya University, Chikusa, Nagoya, 464–8603, Japan

Corresponding Author:
Tsuyoshi Yamaguchi: yamaguchi.tsuyoshi@material.nagoya-u.ac.jp

Graphical Abstract

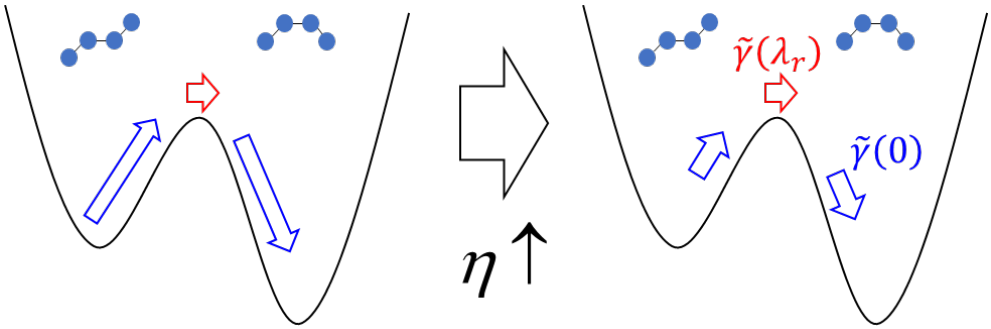

Abstract

The trans–gauche isomerization reaction of model 1,2-dichloroethane in water and ethylene glycol (EG) was studied by molecular dynamics (MD) simulation. With low barrier height, the reaction in EG was slower than that in water, and their difference decreased with increasing barrier height. Compared with the time-dependent diffusion model, in water, the effective diffusion coefficient was almost independent of time, whereas it decreased with time in EG. The trends were reproduced by Langevin dynamics simulation with a time-dependent friction coefficient from MD simulation. The effective diffusion coefficient in water agreed well with the prediction of the Grote–Hynes (GH) theory, whereas for EG, the GH theory overestimated the effective diffusion coefficient. It was suggested that the coupling with the slow structural relaxation of EG slows down the dynamics far from the transition state, which may slow down the overall reaction dynamics when the activation barrier is not high.

Keywords: Dynamic solvent effect; Grote-Hynes theory; Isomerization; Structural relaxation; Viscosity

1. Introduction

Chemical reactions in solutions proceed under both static and dynamic effects of solvents. The static effects refer to the modification of the free energy profile along the reaction coordinate through solvation. When the reaction involves modification of the molecular structure, the solvent exerts friction on the dynamics along the reaction coordinate, which is called the dynamic solvent effect (DSE). An example of such a reaction is the unimolecular isomerization reaction in solution, which has been targeted as a model system for DSE studies [1].

Because shear viscosity governs the friction on macroscopic objects immersed in a liquid, it has been used as a measure of microscopic friction on the reaction dynamics of a solute molecule. Typical experimental studies on DSE have thus included determination of the rate constant of a chosen reaction system at a given temperature in solvents with different viscosity values. The change in solvent viscosity was achieved by changing the solvent species, applying pressure, or adding cosolvents. The rate constant was then correlated with the viscosity, and the decrease in rate constant with viscosity was regarded as a manifestation of DSE.

Early experimental studies on DSEs were performed from the point of view of basic physical chemistry, and simple small molecules were chosen as model reaction systems. Time-resolved spectroscopy using pulsed lasers was a popular experimental technique [1-3], and other methods such as nuclear magnetic resonance spectroscopy [4] and ultrasonic spectroscopy [5] were also used. Typical experimental results were that, although the rate constant, k, decreases with increasing shear viscosity, η_0, their correlation was weaker than the hydrodynamic prediction, $k \propto 1/\eta_0$. The empirical power relation $k \propto \eta_0^{-\alpha}$ was then often used, where α is a positive number smaller than unity [1].

The folding dynamics of protein can be regarded as a unimolecular isomerization reaction in solution. Because of the growing interest in the physico-chemical properties of biological systems in recent decades, experimental data on folding dynamics in various conditions have been accumulated [6-8]. It was found that in solvents of low viscosity the variation in the folding rate is rather weak. The idea of "internal friction" was then proposed, in which the friction along the reaction coordinate is dominated by coupling with other intramolecular degrees of freedom, rather than by the dynamics of solvent molecules [7, 9, 10].

Unimolecular isomerization reaction in solution belongs to activation barrier crossing, for which the most basic theory is, of course, the transition state theory (TST). DSE is not included in TST, that is, the rate constant predicted by TST is independent of the shear viscosity of the solvent.

The Kramers theory is the first step for treating the DSE [11]. This theory regards the crossing of the activation barrier as a motion along the reaction coordinate under the influence of Markovian noise. The stochastic motion along the reaction coordinate becomes overdamped in dense liquids, and the probability distribution of the reactant obeys a simple diffusion equation under external potential. In the Kramers theory, the time development of the diffusion equation is scaled by the diffusion coefficient, and thus the reaction rate is proportional to the diffusion coefficient. Therefore, the Kramers theory predicts the η_0^{-1} dependence of the rate constant if the diffusion coefficient along the reaction coordinate is inversely proportional to the shear viscosity of the neat solvent.

The Grote–Hynes (GH) theory is an extension of the Kramers theory, which describes the rate constant in terms of the time correlation function of the reactive current [12]. In contrast to the Kramers theory, in the GH theory, the friction coefficient along the reaction coordinate depends on frequency. The final expression of the GH theory states that the frequency-independent friction coefficient in the Kramers theory is replaced with the frequency-dependent friction at the reactive frequency, which is related to the curvature of the potential at the transition state. The GH theory can thus be regarded as a non-Markovian generalization of the Kramers theory. An extension of the GH theory to include the slowing down caused by energy diffusion, referred to as "PGH theory", was later proposed by Pollak, Grabert, and Hänggi [13, 14].

The activated barrier crossing has also been a target of computer simulation studies [15]. Early studies were limited to reactions on model potentials under the influence of stochastic noise; however, nowadays, it is possible to perform molecular dynamics (MD) simulation of the unimolecular isomerization reaction in solution, including intramolecular modes other than the reaction coordinate and the microscopic description of solvent molecules [9, 16, 17]. Hridya and Mukherjee performed a computational study that suggested that the insensitiveness of the folding rate of proteins to the shear viscosity of the solvent is ascribed to the frequency-dependent friction coefficient in the GH theory [18].

In some recent computational studies, a popular method to vary the shear viscosity of a solvent, particularly water, is to scale the atomic masses of the solvent [9, 17, 19, 20]. This operation has two advantages; first, the scaling of the shear viscosity against the atomic mass is quite simple, and second, because the static properties of classical equilibrium systems do not depend on the atomic masses, their scaling does not affect the free-energy profile along the reaction coordinate, which is a crucial factor in determining the rate constant. However, we consider that an important point is missing in the atomic-mass scaling method from the viewpoint of the frequency dependence of the friction

coefficient, because it does not reproduce typical changes in the viscoelastic spectra with changing solvent or applying pressure.

Shear viscosity is a dynamic property of liquids, which is given by the time integral of the autocorrelation function of shear stress according to the Kubo–Green theory [21]. The autocorrelation function of the shear stress is usually bimodal in dense liquids. The fast component is assigned to collisional momentum transfer, and the slow component to collective structural relaxation. The shear viscosity exhibits significant variation, amounting to several orders of magnitude, among liquids of different chemical compositions or thermodynamic conditions. The large variation in shear viscosity is almost exclusively ascribed to that of the relaxation time of the slow component, whereas the amplitude of the slow component and the contribution of the fast component change only mildly. By contrast, the scaling of the atomic mass does not affect the relative contributions of the fast and slow components to the shear viscosity.

The time-dependent friction coefficients on the translational diffusion and intramolecular reaction coordinates also consist of fast and slow components. Although there is still discussion on the relation between the macroscopic viscosity and microscopic friction on a solute molecule, it is natural to expect that the spectral shape of the microscopic friction follows that of the shear viscosity if the time-integrated friction coefficient is related to the zero-frequency shear viscosity. In particular, if the viscosity of the solvent is experimentally increased by applying pressure or dissolving cosolvents, the relaxation time of the slow component of the time-dependent friction along the reaction coordinate follows the increase in shear viscosity of the solvent, whereas the fast friction and the amplitude of the slow friction are expected to be almost constant [22, 23].

The predictions of the Kramers and GH theories differ considerably in the reaction rate response to the relaxation time of the slow friction mode [24]. In the Kramers theory, the retardation in relaxation time is reflected in the reaction rate through the time-integrated friction coefficient. The retardation of the slowest relaxation mode thus results in the significant decrease in the rate constant. By contrast, the rate constant predicted by the GH theory is almost independent of the relaxation time of the slowest mode, because the reactive frequency is much higher than the relaxation rate of the slowest mode. Therefore, we believe that computational work on the effect of solvent viscosity on the reaction rate of the unimolecular isomerization would be better performed on systems where an increase in the shear viscosity of the solvent is accomplished through an increase in the relaxation time of the slowest mode of structural relaxation.

In this work, we performed MD simulations on the trans–gauche isomerization reaction of 1,2-dichloroethane (DCE) in water and ethylene glycol (EG). The conformational

equilibrium of 1,2-dihaloethane was regarded as a model system for the study of solvent effects on chemical equilibrium [25], and the kinetics of the isomerization was also investigated experimentally [5]. EG is the simplest diol molecule, with a shear viscosity of 17 mPa s at ambient condition [26]. EG has been used as a typical viscous liquid experimentally, and its high viscosity is ascribed to the slow structural relaxation, as will be shown in this work. For comparison, water was chosen as a non-viscous solvent without slow structural relaxation, in the sense that its viscoelastic relaxation completes almost within 2 ps, as will be shown in Fig. 1. The transition matrix was calculated as a function of time, and the time-dependent effective diffusion coefficient was deduced from comparison with the time-dependent diffusion model, which will be introduced in Sec. 2.3. The effective diffusion coefficients are also compared with the prediction of the GH theory.

2. Theory

2.1. Rate equation and transition matrix

Suppose that the solute of interest takes two different conformations, trans (t) and gauche (g). The chemical rate equation for the time dependence of the concentrations of these isomers is given as

$$\frac{d}{dt}[\mathrm{t}]_t = -k_{\mathrm{gt}}[\mathrm{t}]_t + k_{\mathrm{tg}}[\mathrm{g}]_t, \tag{1}$$

$$\frac{d}{dt}[\mathrm{g}]_t = -k_{\mathrm{tg}}[\mathrm{g}]_t + k_{\mathrm{gt}}[\mathrm{t}]_t, \tag{2}$$

where the rate constants from t to g and from g to t are denoted as k_{gt} and k_{tg}, respectively. The subscript t means that the concentration is the value at time t. The equilibrium constant of the isomerization is related to the rate constants as

$$K \equiv \frac{[\mathrm{g}]_{eq}}{[\mathrm{t}]_{eq}} = \frac{k_{\mathrm{gt}}}{k_{\mathrm{tg}}}, \tag{3}$$

where the subscript *eq* indicates the equilibrium value.

Here we define the transition matrix, $T_{\alpha\gamma}(t)$, where $\{\alpha, \gamma\} = \{\mathrm{t}, \mathrm{g}\}$. $T_{\alpha\gamma}(t)$ denotes the probability that the solute molecule in state γ at time zero is found to be in the state α at time t. When the rate equations, eqs (1) and (2), hold, the relaxation of the transition matrix is given by

$$1 - T_{\mathrm{tg}}(t) - T_{\mathrm{gt}}(t) = \exp[-k_{tot}t], \tag{4}$$

where $k_{tot} \equiv k_{\mathrm{tg}} + k_{\mathrm{gt}}$ means the overall rate constant that governs the relaxation to the equilibrium.

2.2. Dynamics along the reaction coordinate

A unimolecular isomerization reaction is often treated as one-dimensional dynamics along a chosen coordinate *x*, called the "reaction coordinate". The free-energy profile along the coordinate is denoted as $U(x)$. The coordinates perpendicular to *x*, including both intramolecular vibrational modes and solvent degrees of freedom, are projected out. The free-energy profile $U(x)$ possesses two minima separated by an activation barrier. Each minimum corresponds to each isomeric state, and the peak of the activation barrier is called the "transition state".

The dynamics along the reaction coordinate is described by the generalized Langevin equation as

$$m\ddot{x}(t) + \int_0^t d\tau\, \gamma(t-\tau)\dot{x}(\tau) + \frac{\partial U(x(t))}{\partial x} - R(t) = 0, \tag{5}$$

where *m* stands for the effective mass along the reaction coordinate. The time-dependent friction coefficient, $\gamma(t)$, is called the "memory function". Both $\gamma(t)$ and the random force, $R(t)$, describe the effect of the degrees of freedom perpendicular to the reaction coordinate on the dynamics of $x(t)$, and they are related to each other through the fluctuation–dissipation theorem as

$$\gamma(t) = \frac{1}{k_B T} < R(0)R(t) >, \tag{6}$$

where k_B and *T* denote the Boltzmann constant and the absolute temperature, respectively.

The generalized Langevin equation without the potential term is given by

$$m\ddot{x}(t) + \int_0^t d\tau\, \gamma(t-\tau)\dot{x}(\tau) - R(t) = 0, \tag{7}$$

from which the diffusion coefficient along the reaction coordinate, $D_{0,free}$, is obtained as

$$D_{0,free} = \int_0^\infty dt\, Z_{free}(t) = \frac{1}{2}\lim_{t\to\infty}\frac{d}{dt} < |\delta x(t)|^2 >_{free}. \tag{8}$$

The subscript *free* means motion without the potential term. The velocity autocorrelation function, $Z_{free}(t)$, is defined as

$$Z_{free}(t) \equiv < \dot{x}(0)\dot{x}(t) >_{free}, \tag{9}$$

and the definition of the displacement, $\delta x(t)$, is given by

$$\delta x(t) \equiv x(t) - x(0). \tag{10}$$

The diffusion coefficient defined by eq. (8) can be extended to the time-dependent and the frequency-dependent coefficients. The former is defined as

$$D_{free}(t) \equiv \int_0^t d\tau\, Z_{free}(\tau) = \frac{1}{2}\frac{d}{dt} < |\delta x(t)|^2 >_{free}, \tag{11}$$

and the latter as

$$\widetilde{D}_{free}(z) \equiv \int_0^\infty d\tau\, e^{-z\tau} Z_{free}(\tau)\,. \tag{12}$$

According to eq. (7), $\widetilde{D}_{free}(z)$ is related to the memory function as

$$\widetilde{D}_{free}(z) = \frac{k_B T}{mz + \tilde{\gamma}(z)}, \tag{13}$$

where the frequency-dependent friction is defined by

$$\tilde{\gamma}(z) \equiv \int_0^\infty dt\, e^{-zt} \gamma(t). \tag{14}$$

In the frequency regime, where the effect of inertia is negligible ($mz \ll \tilde{\gamma}(z)$) and z is far smaller than the rate of the slowest relaxation of $\gamma(t)$, the diffusion coefficient becomes frequency-independent, and its value is equal to the low-frequency limiting one as

$$\widetilde{D}_{free}(z=0) \equiv D_{0,free} = \frac{k_B T}{\tilde{\gamma}(0)}. \tag{15}$$

The time dependence of $D_{free}(t)$ corresponds to the frequency dependence of $\widetilde{D}_{free}(z)$, that is, the diffusion coefficient is time-dependent if the relaxation of the time-dependent friction coefficient is incomplete.

Under the assumption that the memory function is not affected by the presence of the potential term, we can obtain the time- and the frequency-dependent diffusion coefficients from the MD simulation with a biased potential to cancel $U(x)$. The validity of the assumption will be discussed based on the results of our MD simulation.

2.3. The Kramers theory and the time-dependent diffusion model

The dynamics along the reaction coordinate can be regarded as the time development of the probability distribution of the reaction coordinate and its conjugate momentum. The derivation of the equation for the probability distribution is difficult for the general case with a time-dependent friction coefficient and the effects of inertia. When the friction is Markovian, that is, $\gamma(t) = 2\gamma_0\delta(t)$, and the effects of inertia are negligible, the probability distribution follows the simple Smoluchowski equation as

$$\frac{\partial}{\partial t} P(x,t) = D_0 \frac{\partial}{\partial x}\left[\frac{\partial P(x,t)}{\partial x} + \frac{P(x,t)}{k_B T}\frac{\partial U(x)}{\partial x}\right], \tag{16}$$

where $P(x,t)$ denotes the probability density to find the system at the position x at time t, and $D_0 \equiv k_B T/\gamma_0$ is the diffusion coefficient. Kramers derived the expression of the rate constant, k_{Kr}, from eq. (16) as [11]

$$k_{Kr} \propto \frac{D_0}{\int dx \exp\left(\frac{U(x)}{k_B T}\right)}. \tag{17}$$

The integral in the denominator runs from the reactant to the product, but the contribution around the transition state is dominant due to the large value of $U(x)$. An important point in eq. (17) is that the reaction rate constant is proportional to D_0. Therefore, if we assume that the microscopic friction γ_0 is proportional to the shear viscosity of the solvent, η_0, the reciprocal relation between the shear viscosity and the rate constant is expected.

An extension of the Smoluchowski equation, eq. (16), to include the time dependence of the diffusion coefficient is the time-dependent diffusion model as

$$\frac{\partial}{\partial t} P(x,t) = D(t) \frac{\partial}{\partial x} \left[\frac{\partial P(x,t)}{\partial x} + \frac{P(x,t)}{k_B T} \frac{\partial U(x)}{\partial x} \right]. \tag{18}$$

The time-dependent diffusion model has actually been used to analyse chemical reactions of systems with slow memory [27-30]. An advantage of the time-dependent diffusion model is its relatively easy numerical treatment. By changing the time variable *t* into the effective time *s*, defined as

$$s \equiv \int_0^t D(\tau) d\tau, \tag{19}$$

eq. (18) reduces to the Smoluchowski equation with $D_0 = 1$ as

$$\frac{\partial}{\partial s} P(x,s) = \frac{\partial}{\partial x} \left[\frac{\partial P(x,s)}{\partial x} + \frac{P(x,s)}{k_B T} \frac{\partial U(x)}{\partial x} \right]. \tag{20}$$

2.4. The GH theory

The GH theory deals with a chemical reaction in which the reaction rate is given by the time correlation function of the reactive flux at the transition state [12]. Applying the theory to the activation barrier crossing in solution, Grote and Hynes derived an extension of the Kramers theory to include the frequency dependence of the memory function. The rate constant predicted by the GH theory is given by

$$k_{GH} = \frac{\lambda_r}{\omega_b} k_{TST}, \tag{21}$$

where k_{TST} denotes the reaction rate constant of TST, and ω_b stands for the barrier frequency determined by the curvature at the transition state. The reactive frequency, λ_r, is related to the barrier frequency as follows:

$$\lambda_r = \frac{m\omega_b^2}{m\lambda_r + \tilde{\gamma}(\lambda_r)}. \tag{22}$$

From eqs (13), (21), and (22), k_{GH} is described in terms of the frequency-dependent

diffusion coefficient as

$$\frac{k_{GH}}{k_{TST}} = \frac{m\omega_b}{k_B T}\widetilde{D}_{free}(\lambda_r). \tag{23}$$

By contrast, the rate constant of the Kramers theory is given in the limit of large friction by [11]

$$\frac{k_{Kr}}{k_{TST}} = \frac{m\omega_b}{k_B T} D_{0,free}, \tag{24}$$

where $D_{0,free}$ is the diffusion coefficient in the low-frequency limit given by eq. (15). Therefore, the difference between the Kramers and GH theories is that the dynamics of the barrier crossing is described by the zero-frequency diffusion coefficient in the former, whereas the dynamics is governed by the diffusion coefficient at the reactive frequency in the latter.

3. Computational method

Equilibrium MD simulation runs were performed on systems in which a DCE molecule was dissolved in solvent EG or water. MD simulation runs of neat solvents were also performed to calculate the shear viscosity. All the MD simulation runs were performed using the GROMACS 2019.1 package [31], except for that of neat water, for which GROMACS 5.1.2 was used. The optimized potential for liquid simulation–all atom (OPLS-AA) model was used for DCE [32], the parameters for which were taken from the .itp files within the GROMACS package. A water molecule was described by the extended simple point charge (SPC/E) model [33]. The force field proposed by Szefczyk and Cordeiro was used for EG [34], the parameters of which were taken from the Supporting Information of their paper. The geometric combination rule of the OPLS-AA model was used for the Lennard-Jones (LJ) parameters between different kinds of atoms. The intramolecular geometry of water was fixed by the SETTLE algorithm [35]. The bond lengths involving H atoms, excluding the O–H bond of water, were fixed by the LINCS algorithm [36]. Other bond angles and dihedral angles were treated as flexible.

The solution of DCE in EG consisted of one DCE and 944 EG molecules. The aqueous solution of DCE was composed of one DCE and 2718 water molecules. The neat solvent systems, EG and water, were made of 1000 EG and 2744 water molecules, respectively. In all systems, all the molecules were contained in a cubic cell with periodic boundary condition. The temperature and pressure of the systems were 298 K and 1 bar, which were controlled with a Nosé–Hoover thermostat and a Parrinello–Rahman barostat, respectively [37]. The equation of motion was integrated by the leap-frog algorithm with the time step of 1 fs [37]. The long-range part of the Coulombic interaction was evaluated

using the particle mesh Ewald method with a Fourier spacing of 0.12 nm [38]. The short-range part of the Coulombic interaction and the LJ potential were cut off at 1.2 nm.

The topic of interest in this study was the trans–gauche isomerization reaction of DCE, and the reaction coordinate of the isomerization was chosen simply to be the Cl–C–C–Cl dihedral angle of DCE, denoted as φ. MD simulation runs were also performed with an additional potential on φ in both water and EG to examine the effect of the activation barrier between the trans and gauche states. The functional form of the additional potential is given by

$$\frac{U_{ex}(\varphi)}{k_B T} = \frac{\Delta_{ex}}{2}[1 - \cos 3\varphi]. \tag{25}$$

The values of the excess barrier height, Δ_{ex}, were 0 (no excess barrier), 1, and 3.

For all six solution systems, three values of Δ_{ex} and two solvents, a 20 ns equilibration run was performed first. Next, a 100 ns production run was performed, in which the nuclear coordinates were written at 100 fs intervals. Then, a 1 μs production run was performed with an output interval of 1 ps. The MD simulation run of neat EG was of 1 μs duration, and was preceded by a 100 ns equilibration run. The shear stress was calculated every 10 fs, and saved at 1 ps intervals. The production run of neat water was of 100 ns duration, following a 10 ns equilibration run. The shear stress was calculated every 10 fs, at an output interval of 100 fs.

In both solutions, the equilibrium MD simulation runs were performed with a biased potential that cancels the potential of mean force to obtain the time-dependent diffusion coefficient along the reaction coordinate. In these runs, the probability distribution of the dihedral angle, $P(\varphi)$, was first evaluated from the second production run of Δ_{ex}= 0. The potential of mean force was then fitted into the fifth-order polynomial of $\cos\varphi$ as

$$-k_B T ln\, P(\varphi) \simeq \sum_{n=0}^{5} C_n \cos^n \varphi\,. \tag{26}$$

Then, a 10 ns equilibrium run was performed with the approximated biased potential and the distribution obtained was used to adjust the biased potential. Next, a 100 ns run was performed to adjust the biased potential further. Finally, a 100 ns production run was performed with the adjusted biased potential. The distribution run of the final production run cannot be uniform, because the fifth-order polynomial cannot exactly reproduce the potential of mean force. However, the relative mean-square deviations from the uniform distribution were small, only about 1.5% and 3% for the solutions of water and EG, respectively.

Langevin dynamics (LD) simulations were also performed on both solutions with the

three values of Δ_{ex} based on the generalized Langevin equation, eq. (7). The potentials of mean force were taken from the final production MD runs with the biased potential. The memory function was approximated as a multiexponential one,

$$\gamma(t) = 2\tilde{\gamma}_0\delta(t) + \sum_{n=1} \frac{\tilde{\gamma}_n}{\tau_n} \exp\left(-\frac{t}{\tau_n}\right), \tag{27}$$

where the parameters $\tilde{\gamma}_n$ and τ_n were determined to reproduce $D_{\varphi,free}(t)$ of the final production MD runs. The numbers of the exponential modes were 1 for water and 2 for EG. The exponential memory function was obtained as a coupling with overdamped harmonic oscillators, as proposed by Kappler and co-workers [39, 40]. The integration of the generalized Langevin equation, eq. (7), was performed by using the fourth-order Runge–Kutta method with a time step of 1 fs. The LD simulation run was performed for 110 μs for each system. The initial 10 μs was treated as the equilibration span, and the remaining 100 μs run was used for analysis.

4. Results and discussion

4.1. Translational dynamics

According to the Kubo–Green theory, the shear viscosity of a liquid is related to the time correlation function of the off-diagonal part of the stress tensor, $P_{xy}(t)$, as [21]

$$\eta_0 = \frac{V}{k_B T} \int_0^\infty < P_{xy}(0) P_{xy}(t) > dt, \tag{28}$$

where V stands for the volume of the system. From the analogy of the time-dependent diffusion coefficient, eq. (11), the time-dependent shear viscosity, $\eta(t)$, is defined as

$$\eta(t) \equiv \frac{V}{k_B T} \int_0^t < P_{xy}(0) P_{xy}(\tau) > d\tau. \tag{29}$$

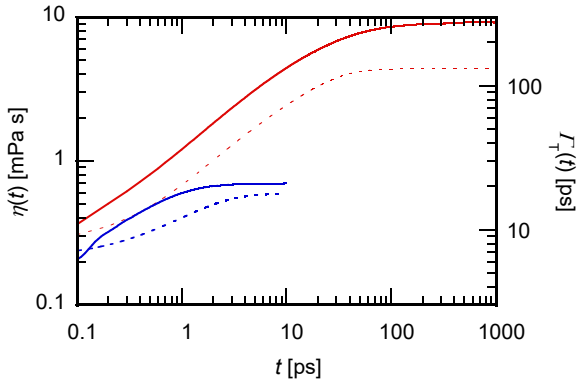

Fig. 1. The time-dependent shear viscosity defined by eq. (29) (solid, left axis) and the running integral of the translational memory function defined by eq. (31) (dotted, right axis). The red and blue curves are the

functions of water and EG, respectively.

The time-dependent shear viscosities of both liquids, determined by the MD runs of neat liquids, are plotted with solid curves in Fig. 1. The long-time limiting values, corresponding to η_0, are 0.70 mPa s for water and 9.2 for EG. These values are in reasonable agreement with previous works using the same potential models [34, 41]. Comparing the time profiles of $\eta(t)$ of both liquids, the difference is slight in the sub-picosecond regime, and the larger-than-water viscosity of EG is ascribed to the slower relaxation time. Wald and Kaatze reported the ultrasonic relaxation time of EG at 298 K as 53 ps [42]. If we regard the relaxation time as that of the shear stress, the shear relaxation of our MD simulation (Fig. 1) is slightly faster than the experimental value, which can explain the fact that the value of η_0 was smaller than the experimental value.

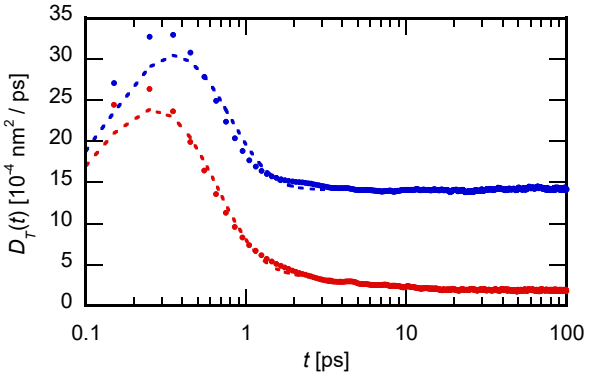

Fig. 2. The time-dependent translational diffusion coefficients of DCE in water (blue) and EG (red). Filled circles show results of MD simulation runs, and the dotted curves are fits obtained using the multiexponential memory functions, eq. (27).

The translational dynamics of DCE in both solvents was analysed by calculating the time-dependent translational diffusion coefficient, $D_{\mathrm{T}}(t)$, which is defined in analogy with eq. (11) as

$$D_T(t) \equiv \frac{1}{6}\frac{d}{dt}\langle|\delta \boldsymbol{r}_{CM}(t)|^2\rangle\,, \tag{30}$$

where $\delta \boldsymbol{r}_{CM}(t) \equiv \boldsymbol{r}_{\mathrm{CM}}(t) - \boldsymbol{r}_{CM}(0)$ stands for the displacement of the centre-of-mass position. The calculation of $D_{\mathrm{T}}(t)$ was performed using the first production runs. The results of the MD simulation are plotted in Fig. 2 with filled circles. Because the results are barely dependent on the values of Δ_{ex}, only the results of $\Delta_{\mathrm{ex}} = 0$ were plotted and analysed.

$D_{\mathrm{T}}(t)$ initially increases proportionally with t, showing a peak around 300 fs; it then decays and finally reaches a constant value corresponding to the translational diffusion coefficient (Fig. 2). The initial rise describes the inertial motion, and the decay is caused by the coupling with the friction of finite relaxation time. The convergence in water is almost completed within 2 ps, whereas the decrease in $D_{\mathrm{T}}(t)$ lasts up to several tens of ps in EG. The slow convergence of $D_{\mathrm{T}}(t)$ in EG appears to correspond to that of $\eta(t)$ in Fig. 1. The diffusion coefficients in the long-time limit are 1.41×10^{-9} m^2/s in water and 1.89×10^{-10} in EG. Their ratio, 7.5, is smaller than that of η_0, 13, but the increase in shear viscosity from water to EG is reflected in the decrease in the translational diffusion coefficient of DCE.

The generalized Langevin equation without an external potential, eq. (7), was applied to the centre-of-mass motion, $\boldsymbol{r}_{\mathrm{CM}}(t)$, to extract the coupling of the translational motion of the solute with the slow structural relaxation of the solvent. The memory function, $\gamma_{\mathrm{T}}(t)$, was approximated as the multiexponential function, eq. (27), and the parameters were optimized to reproduce $D_{\mathrm{T}}(t)$.

The results of the fitting are shown with dotted curves in Fig. 2. The numbers of the exponential functions are 1 for water and 2 for EG, as described in the previous section. The use of additional exponential functions hardly improved the fitting. The agreement between the simulation and the fitting is good after several hundred fs. A discrepancy was observed around the peak at 300 fs, which was probably due to the approximation in eq. (27) that the fastest collisional friction is described as a delta function. The time constant for water was $\tau_1 = 1.4$ ps, and for EG the two constants were $\tau_1 = 2.3$ and $\tau_2 = 16.8$ ps.

The running integrals of $\gamma_{\mathrm{T}}(t)$, defined as

$$\Gamma_T(t) \equiv \int_0^t d\tau \gamma_T(\tau), \tag{31}$$

are plotted in Fig. 1 for comparison with $\eta(t)$. The variation in $\Gamma_T(t)$ between the two solvents follows that of $\eta(t)$ in that the larger friction in EG originates from the slow relaxation time. In particular, the slowest relaxation of $\Gamma_T(t)$ occurs in the same time scale as $\eta(t)$, suggesting that the slow structural relaxation that gives a large shear viscosity of EG is coupled to the translational dynamics of DCE.

4.2. Transition matrix and effective diffusion coefficients

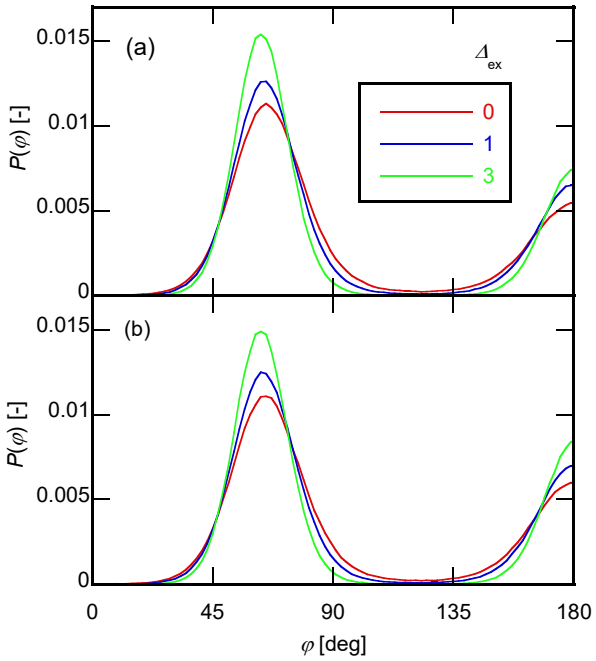

Fig. 3. Probability distribution functions of the dihedral angle of Cl–C–C–Cl of DCE in (a) EG and (b) water. The values of Δ_{ex} are 0 (red), 1 (blue), and 3 (green).

The probability distribution functions determined from the second 1 μs production runs are shown in Fig. 3. The distribution is symmetric about φ = 180°, and only the distributions at 0° < φ < 180° are shown. The distribution functions for the two solvents are close to each other, which means that the static solvent effect on the potential of mean force is small. The distribution shows two peaks at 60° and 180°, which correspond to the gauche and trans states, respectively. The valleys are observed at 0° and 120°, indicating the activation barriers of the isomerization reaction. The former valley is deeper than the latter, because the activation barrier between the two gauche states is higher than that between the gauche and trans states due to the steric hindrance between two Cl atoms. The peak becomes higher and the valley becomes deeper with increasing Δ_{ex}, as expected. We confirmed numerically that the change in the potential of mean force is equal to that in the additional potential, eq. (25) (results not shown for brevity). We class 120° < φ < 240° to belong to the trans state, and the other values are regarded as the gauche state.

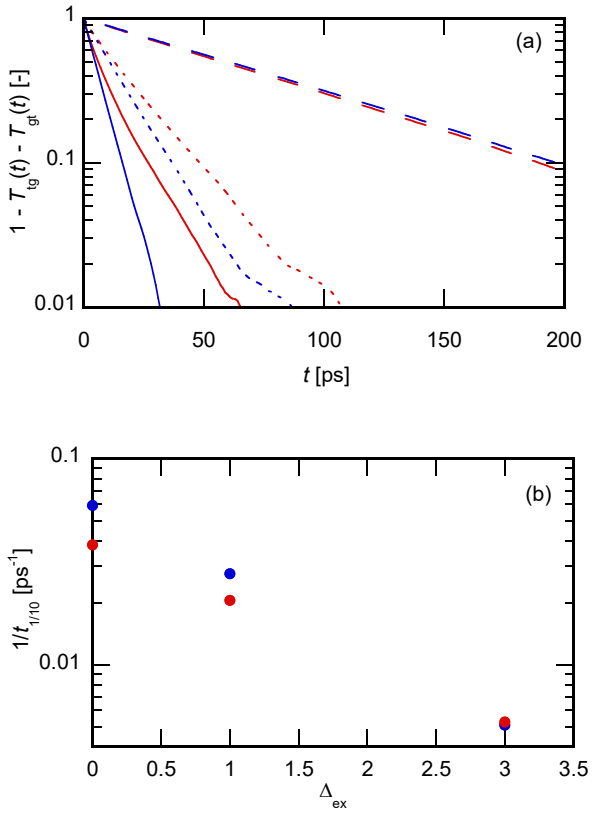

Fig. 4. (a) The transition matrix $1 - T_{tg}(t) - T_{gt}(t)$ in EG (red) and water (blue). The values of Δ_{ex} are 0 (solid), 1 (dotted), and 3 (dashed). (b) The reciprocal reaction time, $1/t_{1/10}$, as the function of Δ_{ex}.

The transition matrices were calculated from the second production runs for all six systems, $\Delta_{ex} = 0$, 1, and 3 in EG and water; $1 - T_{tg}(t) - T_{gt}(t)$ are plotted as a function of time in Fig. 4a. According to eq. (4), this function decays exponentially when the rate equation holds, and the decay rate is equal to the overall rate constant, k_{tot}. In both solvents, the relaxation of the transition matrix becomes slower with increasing additional barrier height, Δ_{ex}, as expected.

The transition matrix decays about twice as slowly in EG as in water at $\Delta_{ex} = 0$. The modification of the potential of mean force by solvent is small (Fig. 3), and thus it is natural to interpret that the retardation of the decay in EG is related to its higher viscosity. The retardation in relaxation for EG becomes smaller with increasing Δ_{ex}, and the reaction proceeds at almost the same rate when $\Delta_{ex} = 3$. Looking closely at the time profiles, the decay of $1 - T_{tg}(t) - T_{gt}(t)$ is almost exponential at $\Delta_{ex} = 3$, as is expected from the rate equation in Sec. 2.1, whereas the slope in Fig. 4a is a slightly decreasing function of time at $\Delta_{ex} = 0$ and 1. The deviation from the exponential function is larger in EG than in water. Comparing in detail the time profiles in EG and water at the same value of Δ_{ex}, their initial

slopes are close to each other, and the slower relaxation in EG is realized by the larger deviation from the exponential function at a longer time. The effective reaction times of the six systems, $t_{1/10}$, were determined as the time of $1 - T_{tg}(t) - T_{gt}(t) = 0.1$, and plotted as the function of Δ_{ex} in Fig. 4b. The increase in $t_{1/10}$ with Δ_{ex} is slower in EG than in water, and the values of $t_{1/10}$ are almost the same in the two solvent at $\Delta_{ex} = 3$.

Based on the time-dependent diffusion model, eq. (18), the transition matrix in Fig. 4a is converted into the time-dependent effective diffusion coefficient, $D_{\varphi,eff}(t)$, in the following manner. First, the potential of mean force, $U(\varphi)$, is calculated from the probability distribution function. Because the distribution function around the activation barrier is noisy due to the small population in the cases of $\Delta_{ex} = 1$ and 3, the $U(\varphi)$ of these systems is evaluated from the $U(\varphi)$ of $\Delta_{ex} = 0$ by adding the additional potential, eq. (25). Then, eq. (20) is solved numerically under $U(\varphi)$ to determine the transition matrix $T_{\alpha\gamma}^{TDD}(s)$ as a function of s. The correspondence between s and t is then given to satisfy

$$1 - T_{tg}^{TDD}\big(s(t)\big) - T_{gt}^{TDD}\big(s(t)\big) = 1 - T_{tg}^{MD}(t) - T_{tg}^{MD}(t), \tag{32}$$

where $T_{\alpha\gamma}^{MD}(t)$ stands for the transition matrix from the MD simulation. Finally, $D_{\varphi,eff}(t)$ is determined according to eq. (19) as

$$D_{\varphi,eff}(t) = \frac{ds(t)}{dt}. \tag{33}$$

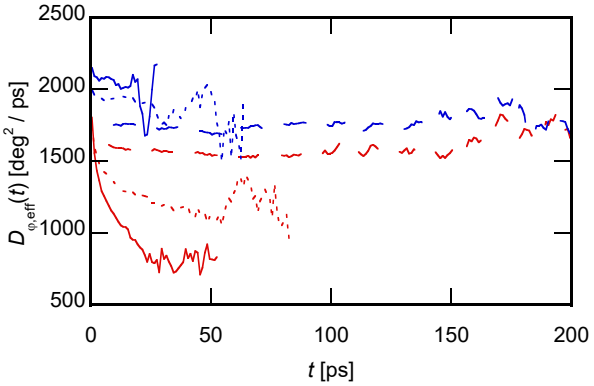

Fig. 5. Time-dependent effective diffusion coefficients in EG (red) and water (blue) determined from MD simulation. The values of Δ_{ex} are 0 (solid), 1 (dotted), and 3 (dashed).

The time-dependent effective diffusion coefficients determined in this way are shown in Fig. 5. The error in $D_{\varphi,eff}(t)$ becomes large at long t, where $1 - T_{tg}^{MD}(t) - T_{tg}^{MD}(t)$ is small, and therefore the plot was truncated at the time t of $1 - T_{tg}^{MD}(t) - T_{tg}^{MD}(t) = 0.02$.

In water, $D_{\varphi,eff}(t)$ is nearly independent of time, as expected. Although the variation is not large, $D_{\varphi,eff}(t)$ appears to decrease with increasing barrier height. By contrast, $D_{\varphi,eff}(t)$ is a decreasing function in EG, and the degree of the decrease becomes smaller with increasing barrier height. The constant $D_{\varphi,eff}(t)$ in Fig. 5 corresponds to the exponential decay of $1 - T_{\mathrm{tg}}^{MD}(t) - T_{\mathrm{tg}}^{MD}(t)$ in Fig. 4a, and the decrease in $D_{\varphi,eff}(t)$ with time results from the deviation from the exponential function.

The time-dependent diffusion model is a theory for treating the diffusion-limited reactions in systems of non-Markovian diffusion. This model assumes that the diffusive dynamics under potential can be described just by introducing the time-dependent diffusion coefficient determined from the mean-square displacement without external potential. However, the results in Fig. 5 suggest that $D(t)$ of the time-dependent diffusion model should also depend on the potential.

4.3. Free diffusion of the dihedral angle

We performed equilibrium MD simulation runs with biased potentials to cancel the potential of mean force to extract the diffusion coefficient for the dihedral angle in the absence of the potential term. Because the potential of mean force removed in the MD simulation with biased potential includes the potential of mean force from solvent molecules, the static solvent effects are eliminated there. By contrast, the DSEs remain, because they are related to the dynamic fluctuation around the average. Before analysing the diffusion coefficient of the biased systems, however, we have to examine the effective mass for the dihedral angle, which appears in the first term of the generalized Langevin equation, eq. (5). Although the mass m is treated as a constant in eq. (5), the effective mass for the dihedral angle depends on the intramolecular coordinates including the dihedral angle itself.

In this work, the dihedral angle-dependent effective mass, $\mu(\varphi)$, is estimated under the approximation that DCE is a molecule composed of four atoms, Cl–C–C–Cl. The mass of the H atoms is small compared with those of C and Cl, and its contribution to $\mu(\varphi)$ is considered to be small. For convenience, we number the terminal Cl atoms as 1 and 4, and the central C atoms as 2 and 3, where the C 2 is bonded with Cl 1. The Cl–C–C–Cl molecule has 12 degrees of freedom. Three of them belong to the centre-of-mass motion, three to the rotation of the whole molecule, three to the bond lengths, two to the C–C–Cl bond angles, and the remaining one to the dihedral angle, φ. Our strategy was to find, for a given intramolecular conformation, the set of the velocities of atoms, $\{\boldsymbol{v}_n\}$, for which the total momentum and the total angular momentum are zero, the time derivatives of the bond lengths and the bond angles are zero, and $\dot{\varphi} = 1$. Then, calculate the kinetic

energy as

$$K = \frac{1}{2}\sum_{n=1}^{4} m_n v_n^2 , \tag{34}$$

where m_n stands for the mass of atom n, and evaluate the mass, μ, for the given conformation, as

$$K = \frac{1}{2}\mu\dot{\varphi}^2 = \frac{1}{2}\mu. \tag{35}$$

It is relatively easy to find the set of velocities, $\{\boldsymbol{v}_n\}$, that satisfy the above conditions. First, set the velocities as

$$\boldsymbol{v}_1 = \boldsymbol{v}_2 = \boldsymbol{v}_3 = 0, \qquad \boldsymbol{v}_4 = \boldsymbol{r}_{34} \times \frac{\boldsymbol{r}_{23}}{|\boldsymbol{r}_{23}|}, \tag{36}$$

where $\boldsymbol{r}_{nn'}$ stands for the position vector from atom n' to n. With this set of velocities, the time derivatives of the bond lengths and the bond angles are zero, but the centre-of-mass momentum and the total angular momentum remain. Then, add the translational and rotational motions to cancel the overall translational and rotational motions.

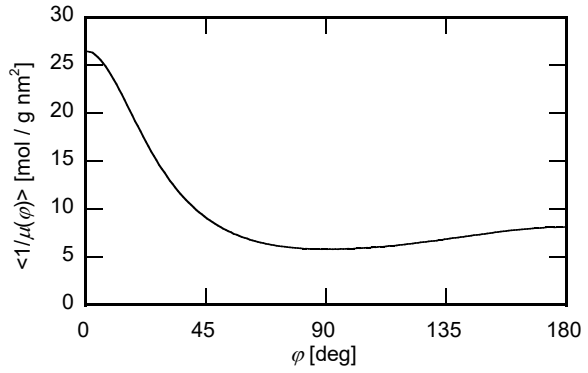

Fig. 6. Reciprocal effective mass for the dihedral angle of DCE in water.

The effective mass for the dihedral angle, $\mu(\varphi)$, was calculated for each conformation of DCE during the simulation run, and the average of its inverse was calculated as a function of φ. The average was performed on the reciprocal mass, because it is related to the initial value of the velocity autocorrelation function of the dihedral angle as $\langle\dot{\varphi}^2\rangle = k_B T\langle 1/\mu(\varphi)\rangle$. The result in water is shown in Fig. 6; the result in EG was almost the same and is omitted here. In Fig. 6, $\mu(\varphi)$ is small around $\varphi = 0°$, because of the increase in the Cl–C–C angles caused by the steric hindrance between two Cl atoms.

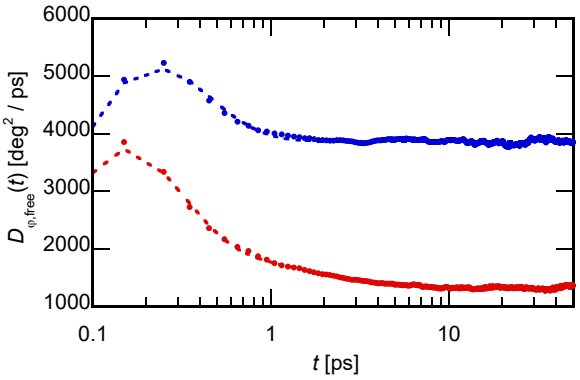

Fig. 7. Time-dependent diffusion coefficients of the dihedral angle without the potential term. The results in EG and water are plotted in red and blue, respectively. Solid circles show the results of the MD simulation, and the dotted lines indicate the fittings using the generalized Langevin equation.

The time-dependent diffusion coefficient of the dihedral angle without the potential term, $D_{\varphi,free}(t)$, was calculated from the mean-square displacement of the dihedral angle in the MD simulation runs with the biased potential as

$$D_{\varphi,free}(t) \equiv \frac{1}{2}\frac{d}{dt}\langle|\varphi(t) - \varphi(0)|^2\rangle. \tag{37}$$

The results in both solvents are shown in Fig. 7. The diffusivity of the dihedral angle is higher in water than in EG, indicating that the larger friction is exerted on the motion of the dihedral angle of DCE in the solvent of higher viscosity, EG. In particular, the results in Fig. 7 contradict the idea of internal friction, i.e., that the friction on the dihedral angle is dominated by the coupling with other intramolecular degrees of freedom rather than the solvent motions. The dominance of the solvent-induced friction over the internal friction appears natural considering the small number of intramolecular degrees of freedom in DCE. The long-time limiting value of $D_{\varphi,free}(t)$ in water is about three times larger than that in EG. The ratio of the diffusion coefficients in the two solvents, 3, is smaller than the corresponding value for the translational diffusion, 7.5. Therefore, the coupling of the motion of the dihedral angle with solvent appears smaller than that of the centre-of-mass motion.

In Fig. 7, $D_{\varphi,free}(t)$ converges to a constant value within 2 ps in water, but a slow decrease with time continues up to 10 ps in EG. This is a similar trend to $D_T(t)$ (Fig. 2), and suggests the presence of the slow relaxation in the time-dependent friction coefficient in EG. To obtain the time-dependent friction on the dihedral angle in both solvents approximately, we applied the generalized Langevin equation to $D_{\varphi,free}(t)$, as was performed on $D_T(t)$. The multiexponential form of the time-dependent friction, eq. (27),

was used, where the numbers of the exponential modes are 1 and 2 for water and EG, respectively. The mass in the generalized Langevin equation was approximated to be a constant, the value of which is equated with the inverse of the average of $\langle 1/\mu(\varphi)\rangle$ over $0° < \varphi < 180°$.

The fittings with the multiexponential friction are displayed in Fig. 7 as dotted curves, which reproduce the results of the MD simulation well. The time constant τ_1 is 480 fs in water, whereas τ_1 = 480 fs and τ_2 = 3.0 ps in EG. These values are several times smaller than the corresponding values for the translational diffusion. We consider that this is partly because the memory associated with the slow structural relaxation of the solvent is lost through the motion of the dihedral angle itself. In the case of EG, for example, the dihedral angle can diffuse about 120° within 10 ps according to the long-time limiting value of $D_{\varphi,free}(t)$. The value of 120° amounts to the distance between the trans and gauche states. Therefore, the dihedral angle of the solute can escape from the potential trap produced by the solvation through the diffusive motion of the dihedral angle. A recent MD study on the translational diffusion of a solute demonstrated that the diffusion coefficient decreases with increasing mass of the solute, which suggests that the memory is partly lost through the motion of the solute [43]. In any case, the motion of the dihedral angle of DCE in EG is coupled to the slow dynamic mode of τ_2 = 3.0 ps, and is considered to be related to the structural relaxation of EG.

4.4. LD simulation and comparison with the GH theory

LD simulations were performed on the six systems of the MD simulation to reduce the complex solute–solvent systems with large numbers of degrees of freedom to simpler ones. The potential of mean force determined by the MD simulation with the biased potential was used as the potential term, and the memory function was taken from that determined from $D_{\varphi,free}(t)$. The results in water were simpler due to the absence of the slow memory, and we discuss the aqueous systems first, followed by the solutions of EG.

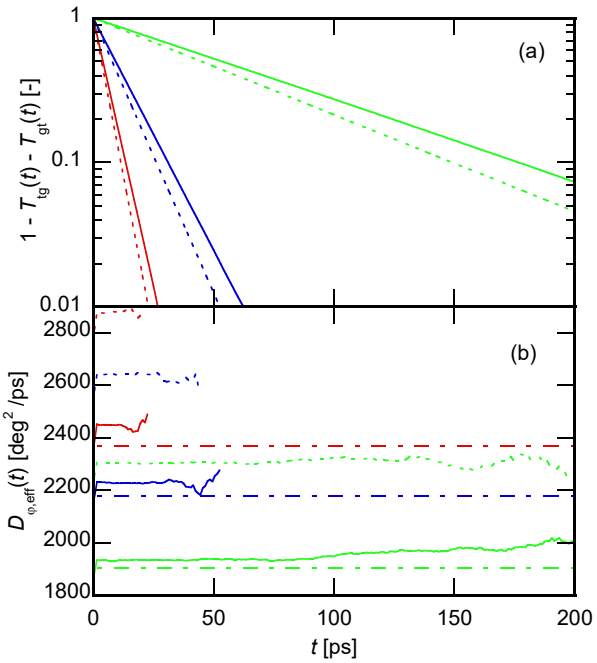

Fig. 8. (a) Transition matrix and (b) time-dependent effective diffusion coefficients for the isomerization reaction of DCE in water calculated by LD simulation. The values of Δ_{ex} are 0 (red), 1 (blue) and 3 (green). The dotted lines show the results using the effective mass averaged over the whole dihedral angle, and the solid lines are obtained with the effective mass at the transition state. The horizontal dash-dotted lines in (b) indicate the prediction of the GH theory.

The results of the LD simulation in water using the reciprocal effective mass averaged over the whole φ region are shown as the dotted curves in Fig. 8. The transition matrices $1 - T_{\mathrm{tg}}(t) - T_{\mathrm{gt}}(t)$ are plotted in Fig. 8a, and the time-dependent effective diffusion coefficients determined by comparison with the time-dependent diffusion model are given in Fig. 8b. The reaction becomes slower with increasing barrier height, as expected; the effective diffusion coefficient $D_{\varphi,eff}(t)$ is almost time-independent, and $D_{\varphi,eff}(t)$ decreases slightly with increasing barrier height. These tendencies are in good agreement with those of the MD simulation (Figs 4 and 5). However, when comparing the absolute values of $D_{\varphi,eff}(t)$ by the MD simulation (Fig. 5) and the LD simulation (Fig. 8b), we see that the former is smaller than the latter.

The dynamics around the transition state plays a crucial role in activated barrier crossing. The parameters in the generalized Langevin equation should thus be determined to reproduce the dynamics around the transition state. Instead of using the reciprocal effective mass integrated over the whole φ region, therefore, we performed the LD simulation with the effective mass at the transition state, φ = 120°. In these LD

simulations, the parameters for the effective friction, $\tilde{\gamma}_n$ and τ_n, determined in the previous subsection were used without modification (Fig. 8, solid curves). The reaction becomes a little slower by varying the value of the effective mass. In particular, the absolute values of $D_{\varphi,eff}(t)$ now approach those of the MD simulation (Fig. 5). The decrease in reaction rate with increasing effective mass means that the barrier-crossing dynamics cannot be regarded as diffusive. The results of the LD simulation remain slightly larger than those of the MD simulation, which might be because the friction coefficient is dependent on the dihedral angle.

Comparing eqs (23) and (24), the diffusion coefficient at the reactive frequency, $\widetilde{D}_{free}(\lambda_r)$, can be regarded as the effective diffusion coefficient predicted by the GH theory. In Fig. 8b, $\widetilde{D}_{free}(\lambda_r)$ from the GH theory is calculated and compared with $D_{\varphi,eff}(t)$ from the LD simulation. The effective mass at the transition state is used as the mass in eq. (22), and the multiexponential approximation from the MD simulation with the biased potential is used as the frequency-dependent friction, $\tilde{\gamma}(z)$. The values of the barrier frequency, ω_b, are 16.4, 18.4, and 21.9 ps^{-1} for Δ_{ex} = 0, 1, and 3, respectively, which are determined from the potential of mean force from the biased MD simulation. The results of the LD simulation are reproduced well by the GH theory in Fig. 8b. In particular, the weak decrease in the effective diffusion coefficient with increasing barrier height is described by the GH theory.

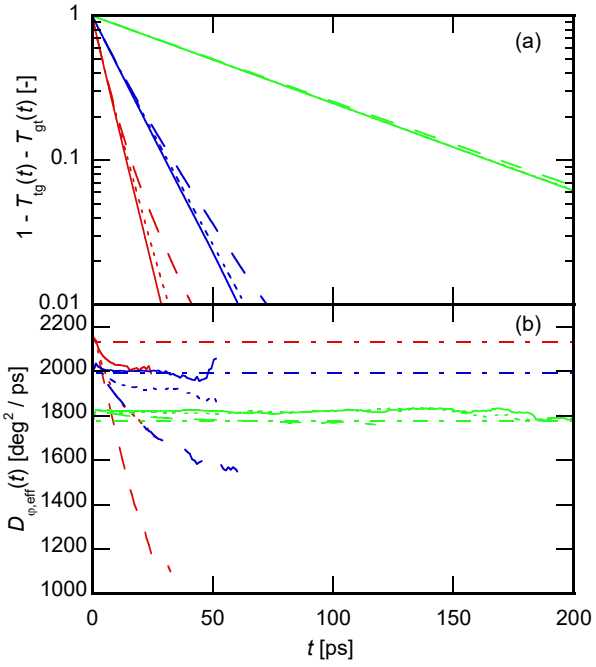

Fig. 9. (a) Transition matrix and (b) time-dependent effective diffusion coefficients for the isomerization

reaction of DCE in EG calculated by LD simulation. The values of Δ_{ex} are 0 (red), 1 (blue), and 3 (green). The results with the slowest relaxation time of the memory function, τ_2 = 3.0, 6.1, and 15.2 ps, are shown with the solid, dotted, and dashed curves, respectively. The horizontal dash-dotted lines in (b) indicate the prediction of the GH theory for τ_2 = 3.0 ps.

The results of LD simulation for the EG solutions are shown in Fig. 9. In these simulation runs, the effective mass at the transition state was used. The transition matrix and the time-dependent effective diffusion coefficients are shown in Fig. 9a and b, respectively. Contrary to the corresponding functions in water, $D_{\varphi,eff}(t)$ is a decreasing function of time, as observed in the MD simulation (Fig. 5). The decrease of $D_{\varphi,eff}(t)$ in the LD simulation was smaller than that in the MD simulation. The amount of the decrease becomes smaller with increasing barrier height, as observed in the MD simulation.

The predictions of the effective diffusion coefficient by the GH theory are also shown in Fig. 9b for comparison. $D_{\varphi,eff}(t)$ is close to the theoretical prediction at the initial time, and the downward deviation becomes larger with increasing time. Therefore, the GH theory overestimates the overall rate constant, because it cannot capture the decrease in the effective diffusion coefficient in the long-time regime.

We performed LD simulations in which the time constant of the slowest relaxation, τ_2, was artificially increased from 3.0 to 6.1 and 15.2 ps to examine the effects of the slow structural relaxation on activated barrier crossing in ideal systems. The latter two values were chosen by multiplying the original τ_2 by the factors 2 and 5. The amplitude of the slowest mode in the time domain, $\tilde{\gamma}_2/\tau_2$, was kept constant with increasing τ_2. The other parameters associated with the faster modes, effective mass, and the potential of mean force were also unchanged. Because τ_2 is already much slower than the reciprocal barrier frequency, that is, $\omega_b\tau_2 \gg 1$, the prediction by the GH theory is almost independent of τ_2. By contrast, the increase in $\tilde{\gamma}_2$, proportional to τ_2, enhances the zero-frequency friction, $\tilde{\gamma}(0)$, which leads to the retardation of the reaction in the Kramers theory.

The results of LD simulation with changing τ_2 are also shown in Fig. 9. The time-dependent transition matrix demonstrates that the retardation of the reaction actually occurs with increasing τ_2, in contrast to the prediction of the GH theory. The effect of τ_2 decreases with increasing barrier height. A close examination of the time profiles of Δ_{ex} = 0 and 1 shows that the initial slopes are almost independent of τ_2, and the deviation from the exponential function becomes larger at larger τ_2. The change in $1 - T_{tg}(t) - T_{gt}(t)$ with increasing τ_2 in Fig. 9a is similar to the difference in the MD simulations of the solutions of EG and water in Fig. 4a. It is thus suggested that the slow structural

relaxation of EG is actually coupled to the isomerization of DCE to retard the reaction dynamics.

The time-dependent effective diffusion coefficients, $D_{\varphi,eff}(t)$, also change with τ_2 (Fig. 9b). The initial values are almost independent of τ_2, and they are close to the predictions of the GH theory. The decrease in time increases with increasing τ_2 and decreases with Δ_{ex}.

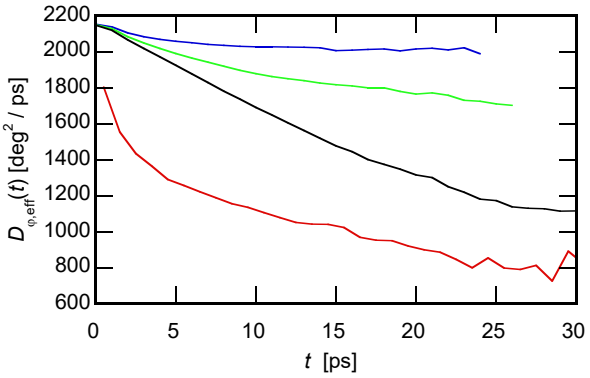

Fig. 10. Time-dependent effective diffusion coefficients for Δ_{ex} = 0 in EG. The result of MD simulation (red) is compared with those of LD simulation with τ_2 = 3.0 ps (blue), 6.1 ps (green), and 15.2 ps (black).

For EG, the results of LD simulation at Δ_{ex} = 0 are compared with those of MD simulation in Fig. 10. $D_{\varphi,eff}(t)$ of the LD simulation of τ_2 = 15.2 ps is closer to the MD simulation than that of τ_2 = 3.0 ps. The time constant of the slowest friction mode on the translational diffusion is 16.8 ps as described in Sec. 4.1. Thus, it is plausible that the τ_2 of the friction on the dihedral angle is as slow as that on the centre-of-mass motion. As discussed in Sec. 4.3, τ_2 of the friction on the dihedral angle might be made smaller in the MD simulation with the biased potential by the free diffusive motion of the dihedral angle itself. Recent MD simulation studies on the position-dependent diffusion coefficient demonstrated that the diffusion coefficient becomes smaller when the tagged molecule is trapped within a potential well [44]. The isomerization reaction of DCE in this work occurs in the presence of potential wells that trap the solute within either the trans or the gauche states. Therefore, the relaxation time of the friction may be larger and the diffusion coefficient may be smaller than the corresponding values of free diffusion of the dihedral angle realized by the MD simulation with the biased potential.

4.5. Dynamics far from the transition state

The remaining question in this work is to determine how the slow friction mode retards

the reaction dynamics of the activated barrier crossing, although the GH theory predicts that the reaction rate constant is insensitive to the time constant of the slow friction. We first examine the possibility that the retardation of the dynamics is caused by the slow energy diffusion.

Straub and co-workers performed LD simulation of the activated barrier crossing with a single exponential memory function, and found that the reaction was retarded with increasing the relaxation time of the memory function [40]. Kappler and co-workers performed LD simulations of similar systems extensively, and demonstrated that the results can be reproduced by the PGH theory [45]. The analysis based on the PGH theory showed that the retardation of the barrier crossing with increasing the memory time is ascribed to the slow energy diffusion. Since the bath mode behave elastically when its relaxation time is long, it cannot provide sufficient dissipation for energy diffusion. One may consider that the retardation of the reaction with increasing τ_2 in this work may also be explained by the slow energy diffusion.

An important difference between the previous works above and our present LD simulation on DCE in EG is, however, that both fast and slow friction modes are present in the latter. The relaxation time of the slow mode is increased while the fast mode is kept constant. If the fast mode provides sufficient energy dissipation, the loss of the dissipation due to the elastic response of the slow mode cannot lead to the energy-diffusion limited regime. In Appendix, we estimated the energy dissipation due to the Markovian mode, $\tilde{\gamma}_0$, based on the PGH theory, and showed that the Markovian friction is sufficiently strong. Since the solute-solvent collisional interaction is always present in viscous solvents, our model with the fast friction mode is considered more realistic.

We then would like to present the two-step models proposed by some researchers as a possible explanation for the retardation of the barrier crossing with increasing τ_2 [46-48]. The overall rate constant of two-step models, k, is described as that of a series reaction as

$$k^{-1} = k_{bc}^{-1} + k_f^{-1}. \tag{38}$$

The rate constant in the first term, k_{bc}, stands for the genuine rate constant of the barrier crossing. The second process, k_f, is assigned to the fluctuation of the solvation structure in the model of Sumi [46], while it corresponds to the diffusion from/to the transition state in the model of Murarka and co-workers [48]. The former process, k_{bc}, is considered to be the rate-determining step in TST, because the population at the transition state is very low. However, the situation may be different when the viscosity of the solvent becomes large. The barrier-crossing dynamics depends on the solvent viscosity only weakly according to the GH theory, because the barrier-crossing dynamics feels only the high-frequency portion of the frequency-dependent friction. By contrast, the fluctuation of the

solvation structure is retarded in viscous solvents. The diffusion from/to the transition state feels the full friction at the zero frequency, which is also expected to follow the zero-frequency shear viscosity of the solvent. Therefore, the latter reaction, k_f, may also contribute to retard the overall reaction to reveal the viscosity dependence of the overall rate constant.

The scenario explains the results of our MD and LD simulations that the retardation of the reaction by the slow friction decreases with increasing barrier height. Because the barrier-crossing reaction is sufficiently slow when the barrier is high, it remains the rate-determining step even in solvents of high viscosity.

The two-step model can explain the viscosity dependence of the rate constant of the internal friction model in a different way. The internal friction model describes the overall rate constant as [7, 9, 10]

$$k^{-1} \propto \sigma + \eta_0, \tag{39}$$

where the viscosity-independent constant, σ, is assigned to the internal friction. In the two-step model, the first term of eq. (38), k_{bc}^{-1}, hardly depends on viscosity because the slow friction mode is decoupled from the barrier crossing, and the second term, k_f^{-1}, is expected to be proportional to η_0 when the isomerizing group is much larger than the solvent size, as is the case of protein folding. Therefore, the viscosity dependence of the rate constant predicted by eq. (38) becomes equivalent to that of eq. (39), although their physical meanings are quite different.

In the following, we examine the time-dependent probability distribution function of the dihedral angle taking the trans–gauche reaction as an example. The probability distribution function at time t under the condition that the solute is in the trans state at time $t = 0$ is defined as

$$\frac{1}{360} P_{\mathrm{t}}(\varphi'; t) d\varphi' \equiv \langle \delta(\varphi(t) - \varphi') f_{\mathrm{t}}\big(\varphi(0)\big) \rangle, \tag{40}$$

where the function $f_{\mathrm{t}}(\varphi)$ is unity when $120° < \varphi < 240°$, and zero otherwise. The distribution function above can be evaluated using equilibrium simulations. We have proposed a similar reweighting method to calculate the transient spectra from equilibrium MD simulations [49]. The distribution in the gauche region is examined after the normalization by $T_{\mathrm{gt}}(t)$.

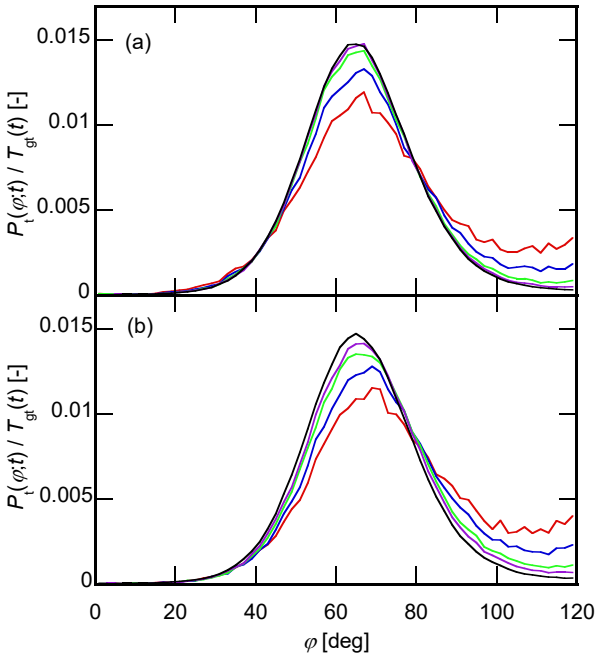

Fig. 11. Conditional probability distribution functions in (a) water and (b) EG obtained by MD simulation. The values of times are 1 (red), 2 (blue), 5 (blue), and 10 ps (purple), respectively. The long-time limiting distributions are also drawn with the black curves.

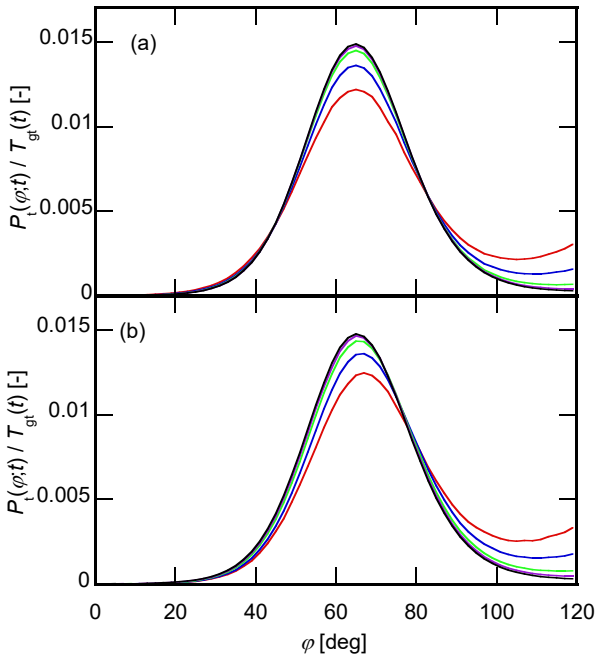

Fig. 12. Conditional probability distribution functions in (a) water and (b) EG obtained by LD simulation. The result of τ_2 = 3.0 ps is shown in panel (b). The values of times are 1 (red), 2 (blue), 5 (blue), and 10 ps

(purple), respectively. The long-time limiting distributions are also drawn with the black curves.

The conditional probability distribution functions from the MD and LD simulations are shown in Figs 11 and 12, respectively. The value of Δ_{ex} is zero in all the results presented in these figures, and the result of EG solution with τ_2 = 3.0 ps is plotted in Fig. 12b. The long-time limiting distributions are calculated from the equilibrium distribution functions. In both figures, the results in water and EG are plotted in panels (a) and (b), respectively, for comparison. The noise of the MD simulation is higher than that of the LD simulation because of the difference in the lengths of simulation runs.

The marked difference between the results in water and EG is the time development of the peak position in both MD and LD simulations. The peak of the transient distribution remains at the peak of the equilibrium distribution in water. By contrast, the peak of the transient distribution in EG deviates from that of the equilibrium distribution to the direction of the transition state, and the peak relaxes slowly to the equilibrium position in the time scale of several picoseconds. The slow diffusion within the product state was also reported in the Stochastic simulation performed by Straub and co-workers when the relaxation of the memory function was slow [40].

The presence of the slow peak shift in EG corresponds to the situation considered by Murarka and co-workers [48]. The diffusion from the transition state to the product gauche state proceeds under the full friction with slow memory. After passing over the barrier, a backward force from the solvent acts on the solute because the solvation structure is optimized for the initial trans state, and the transient stable position of the dihedral angle approaches from the equilibrium gauche toward the initial trans state. In the case of water, because the relaxation of the solvation structure is fast, the diffusion after the barrier crossing is subject only to fast and weak friction, and the distribution within the product state relaxes rapidly to the equilibrium state.

In the present model, the reaction from the trans to the gauche states begins from the equilibrium probability distribution of the reactant state with no population in the product state. Therefore, the barrier crossing governs the reaction initially, which explains that the values of $D_{\varphi,eff}(t)$ in both solvents are close to the prediction of the GH theory (Figs 8b and 9b). In EG, the depletion and the excess population occur in the reactant and the product states, respectively, around the transition state due to the slow diffusion within both states, which reduces $D_{\varphi,eff}(t)$ with increasing time (Fig. 9b).

The variation in the rate-determining step with time in EG is reflected in the decrease in $D_{\varphi,eff}(t)$ with time, which is then related to the non-exponential decay of the transition matrix. The time profile of the transition matrix corresponds to the population

decay in time-resolved laser spectroscopy. Therefore, a detailed analysis of the experimental time profiles obtained by ultrafast spectroscopy should provide information on the reaction mechanisms in viscous solvents. Chemical reactions in viscous solvents, including room-temperature ionic liquids and concentrated organic electrolyte solutions, are now drawing the attention of many researchers, and we hope that the knowledge obtained in this work will help in the understanding of these chemical processes.

5. Summary

The trans–gauche isomerization reaction of DCE in water and EG was studied by MD and LD simulations. The reaction was slower in the more viscous solvent, EG, and the difference between the two solvents became smaller with increasing barrier height. The MD simulation with a biased potential demonstrated that the slow structural relaxation that gives higher viscosity of EG is also coupled to the intramolecular dynamics of the dihedral angle of DCE. According to the GH theory, the slow frictional mode is loosely coupled to the barrier crossing because the reactive frequency is much faster than the structural relaxation. By contrast, the diffusive motion within the reactant and the product states is coupled to the slow friction. Therefore, the role of the former as the rate-determining step is not exclusive when the activation barrier is not very high and the contribution of the slow relaxation to the total friction is large. The effects of the population distribution within the reactant and the product states due to the slow friction occur in the long-time regime, which results in a non-exponential population decay and a decrease in the effective diffusion coefficient with time.

Conflicts of interest

There are no conflicts of interest to declare.

Acknowledgments

The author is grateful to Prof. Y. Kimura (Doshisha University) for valuable discussion, and to Prof. N. Yoshii (Nagoya University) for the use of computational facilities. This work was supported by JSPS KAKENHI (Grant Numbers 19K03768 and 19H02677).

Appendix: Estimation of the energy dissipation by the Markovian friction

The PGH theory provides the correction of the barrier crossing rate given by the GH theory, k_{GH}, due to the slow energy diffusion as [13, 14]

$$\frac{k_{PGH}}{k_{GH}} = \Gamma(\delta), \tag{A1}$$

where $\Delta E \equiv k_B T\delta$ stands for the energy dissipation of the trajectory at the energy of the transition state. The function $\Gamma(\delta)$ is given by

$$\Gamma(\delta) = \exp\left[\frac{1}{2\pi}\int_{-\infty}^{\infty} dx \frac{\ln\left\{1 - e^{-\delta\left(x^2+\frac{1}{4}\right)}\right\}}{x^2+\frac{1}{4}}\right]. \tag{A2}$$

When the energy dissipation is sufficiently strong, $\delta \gg 1$, $\Gamma(\delta)$ rapidly approaches to unity as

$$\Gamma(\delta) \simeq 1 - \frac{2}{\sqrt{\pi\delta}} e^{-\delta/4}, \tag{A3}$$

and k_{PGH} approaches to k_{GH}.

The evaluation of the energy loss, ΔE, in the PGH theory is quite complicated in general, because one have to consider the trajectory along the normal coordinate including the slow bath modes. When the friction is Markovian, however, the trajectory to be considered becomes simply the uncoupled dynamics on the original potential. In our LD simulation on DCE in EG, we approximated the memory function as a sum of one Markovian mode and two exponential modes. In this Appendix, we estimate the energy dissipation due to the first Markovian mode, neglecting the two exponential modes.

In the Markovian case, the energy loss in the PGH theory is described as [14]

$$\Delta E = \int_{-\infty}^{\infty} dt\, \tilde{\gamma}_0 \dot{\theta}^2(t), \tag{A4}$$

where $\theta(t)$ is the friction-free trajectory that starts at the transition state at $t = -\infty$ with zero velocity, passes through the well of the reactant state, and returns to the transition state at $t = \infty$. The calculation using eq. (A4) is relatively easy. The substitution of the parameters used for our LD simulation of DCE in EG with $\Delta_{ex} = 0$ gives the value of $\delta \cong 17$ for the trans state, yielding $\Gamma(\delta) = 0.997$ based on eq. (A3). Therefore, the energy dissipation due to the Markovian friction is sufficiently large in our LD simulation, and the slowing down of the barrier crossing due to the limitation of the energy diffusion is not considered to be plausible.

References

[1] G.R. Fleming, S.H. Courtney, M.W. Balk, Activated barrier crossing: Comparison of experiment and theory, J. Stat. Phys. 42 (1986) 83-104.

[2] M. Lee, A.J. Bain, P.J. McCarthy, C.H. Han, J.N. Haseltine, A.B. Smith, R.M. Hochstrasser, Picosecond photoisomerization and rotational reorientation dynamics in solution, J. Chem. Phys. 85 (1986) 4341-4347.

[3] G. Maneke, J. Schroeder, J. Troe, F. Voß, Picosecond-Absorption Study of the Photoisomerization of Trans-Stilbene in Compressed Gases and Liquids, Berichte der Bunsengesellschaft für physikalische Chemie 89 (1985) 896-906.

[4] D.L. Hasha, T. Eguchi, J. Jonas, High-pressure NMR study of dynamical effects on conformational isomerization of cyclohexane, J. Am. Chem. Soc. 104 (1982) 2290-2296.

[5] S. Koda, A. Iwasawa, H. Hirao, H. Nomura, Ultrasonic investigation of the viscosity dependence of the rate constants of rotational isomerism of dibromoethane and dibromopropane in solution, J. Chem. Soc., Faraday Trans. 91 (1995).

[6] D. Beece, L. Eisenstein, H. Frauenfelder, D. Good, M.C. Marden, L. Reinisch, A.H. Reynolds, L.B. Sorensen, K.T. Yue, Solvent viscosity and protein dynamics, Biochemistry 19 (1980) 5147-5157.

[7] A. Ansari, C.M. Jones, E.R. Henry, J. Hofrichter, W.A. Eaton, The role of solvent viscosity in the dynamics of protein conformational changes, Science 256 (1992) 1796-1798.

[8] G.S. Jas, W.A. Eaton, J. Hofrichter, Effect of Viscosity on the Kinetics of α-Helix and β-Hairpin Formation, J. Phys. Chem. B 105 (2001) 261-272.

[9] D. de Sancho, A. Sirur, R.B. Best, Molecular origins of internal friction effects on protein-folding rates, Nat. Commun. 5 (2014) 4307.

[10] S.A. Pabit, H. Roder, S.J. Hagen, Internal friction controls the speed of protein folding from a compact configuration, Biochemistry 43 (2004) 12532-12538.

[11] H.A. Kramers, Brownian motion in a field of force and the diffusion model of chemical reactions, Physica 7 (1940) 284-304.

[12] R.F. Grote, J.T. Hynes, The stable states picture of chemical reactions. II. Rate constants for condensed and gas phase reaction models, J. Chem. Phys. 73 (1980) 2715-2732.

[13] E. Pollak, H. Grabert, P. Hänggi, Theory of activated rate processes for arbitrary frequency dependent friction: Solution of the turnover problem, J. Chem. Phys. 91 (1989) 4073-4087.

[14] E. Pollak, Classical and Quantum Rate Theory for Condensed Phases, in: S.D. Schwartz (Ed.), Theoretical Methods in Condensed Phase Chemistry, Kluwer, Dordrecht, 2002, pp. 1-46.

[15] J.E. Straub, M. Borkovec, B.J. Berne, Molecular dynamics study of an isomerizing diatomic in a Lennard - Jones fluid, J. Chem. Phys. 89 (1988) 4833-4847.

[16] S.Z. Wan, Y.W. Xu, C.X. Wang, Y.Y. Shi, Analysis of friction kernels for n - butane isomerization in water by the generalized Langevin equation, J. Chem. Phys. 102 (1995) 4976-4980.
[17] J.O. Daldrop, J. Kappler, F.N. Brunig, R.R. Netz, Butane dihedral angle dynamics in water is dominated by internal friction, Proc. Natl. Acad. Sci. U. S. A. 115 (2018) 5169-5174.
[18] V.M. Hridya, A. Mukherjee, Probing the Viscosity Dependence of Rate: Internal Friction or the Lack of Friction?, J. Phys. Chem. B 122 (2018) 9081-9086.
[19] R. Walser, W.F. van Gunsteren, Viscosity dependence of protein dynamics, Proteins: Structure, Function, and Bioinformatics 42 (2001) 414-421.
[20] J. Perkins, E. Edwards, R. Kleiv, N. Weinberg, Molecular dynamics study of reaction kinetics in viscous media, Mol. Phys. 109 (2011) 1901-1909.
[21] J.-P. Hansen, I.R. McDonald, Theory of Simple Liquids, 2nd ed., London, Academic Press, 1986.
[22] N. Shental, E. Rabani, Mode-coupling theory for reaction dynamics in liquids, J. Chem. Phys. 120 (2004) 6642-6647.
[23] R. Biswas, B. Bagchi, Activated barrier crossing dynamics in slow, viscous liquids, J. Chem. Phys. 105 (1996) 7543-7549.
[24] B. Bagchi, D.W. Oxtoby, The effect of frequency dependent friction on isomerization dynamics in solution, J. Chem. Phys. 78 (1983) 2735-2741.
[25] M. Kato, I. Abe, Y. Taniguchi, Raman study of the trans–gauche conformational equilibrium of 1,2-dichloroethane in water: Experimental evidence for the hydrophobic effect, J. Chem. Phys. 110 (1999) 11982-11986.
[26] J.A. Riddich, W.B. Bunger, T.K. Sakano, Organic Solvents, 4th ed., John Wiley & Sons, New York, 1986.
[27] R.A. Denny, B. Bagchi, Barrierless Isomerization Dynamics in Viscous Liquids: Decoupling of the Reaction Rate from the Slow Frictional Forces, J. Phys. Chem. A 103 (1999) 9061-9071.
[28] S. Okuyama, D.W. Oxtoby, The generalized Smoluchowski equation and non - Markovian dynamics, J. Chem. Phys. 84 (1986) 5824-5829.
[29] J.M. Haugh, Analysis of reaction-diffusion systems with anomalous subdiffusion, Biophys. J. 97 (2009) 435-442.
[30] J. Wu, K.M. Berland, Propagators and time-dependent diffusion coefficients for anomalous diffusion, Biophys. J. 95 (2008) 2049-2052.
[31] M.J. Abraham, T. Murtola, R. Schulz, S. Páll, J.C. Smith, B. Hess, E. Lindahl, GROMACS: High performance molecular simulations through multi-level parallelism from laptops to supercomputers, SoftwareX 1-2 (2015) 19-25.
[32] W.L. Jorgensen, N.A. McDonald, M. Selmi, P.R. Rablen, Importance of Polarization for

Dipolar Solutes in Low-Dielectric Media: 1,2-Dichloroethane and Water in Cyclohexane, J. Am. Chem. Soc. 117 (1995) 11809-11810.
[33] H.J.C. Berendsen, J.R. Grigera, T.P. Straatsma, The missing term in effective pair potentials, J. Phys. Chem. 91 (1987) 6269-6271.
[34] B. Szefczyk, M.N. Cordeiro, Physical properties at the base for the development of an all-atom force field for ethylene glycol, J. Phys. Chem. B 115 (2011) 3013-3019.
[35] S. Miyamoto, P.A. Kollman, Settle: An analytical version of the SHAKE and RATTLE algorithm for rigid water models, J. Comput. Chem. 13 (1992) 952-962.
[36] B. Hess, H. Bekker, H.J.C. Berendsen, J.G.E.M. Fraaije, LINCS: A linear constraint solver for molecular simulations, J. Comput. Chem. 18 (1997) 1463-1472.
[37] M.P. Allen, D.J. Tildesley, Computer Simulation of Liquids, Clarendon Press, Oxford, 1987.
[38] U. Essmann, L. Perera, M.L. Berkowitz, T. Darden, H. Lee, L.G. Pedersen, A smooth particle mesh Ewald method, J. Chem. Phys. 103 (1995) 8577-8593.
[39] J. Kappler, V.B. Hinrichsen, R.R. Netz, Non-Markovian barrier crossing with two-time-scale memory is dominated by the faster memory component, Eur. Phys. J. E Soft Matter 42 (2019) 119.
[40] J.E. Straub, M. Borkovec, B.J. Berne, Non - Markovian activated rate processes: Comparison of current theories with numerical simulation data, J. Chem. Phys. 84 (1986) 1788-1794.
[41] S. Balasubramanian, C.J. Mundy, M.L. Klein, Shear viscosity of polar fluids: Molecular dynamics calculations of water, J. Chem. Phys. 105 (1996) 11190-11195.
[42] E. Wald, U. Kaatze, Chain dynamics of ethylene oxide oligomer melts. An ultrasonic spectroscopy study, J. Phys. Chem. B 118 (2014) 13300-13311.
[43] J.O. Daldrop, R.R. Netz, Mass-Dependent Solvent Friction of a Hydrophobic Molecule, J. Phys. Chem. B 123 (2019) 8123-8130.
[44] J.O. Daldrop, B.G. Kowalik, R.R. Netz, External Potential Modifies Friction of Molecular Solutes in Water, Phys. Rev. X 7 (2017) 041065.
[45] J. Kappler, J.O. Daldrop, F.N. Brunig, M.D. Boehle, R.R. Netz, Memory-induced acceleration and slowdown of barrier crossing, J. Chem. Phys. 148 (2018) 014903.
[46] H. Sumi, Theory on reaction rates in nonthermalized steady states during conformational fluctuations in viscous solvents, J. Phys. Chem. 95 (1991) 3334-3350.
[47] T. Asano, K. Matsuo, H. Sumi, Effects of Solvent Fluctuations on the Rate of the ThermalZ/EIsomerization ofN-Benzylideneanilines in a Highly Viscous Liquid Hydrocarbon, Bull. Chem. Soc. Jpn. 70 (1997) 239-244.
[48] R.K. Murarka, S. Bhattacharyya, R. Biswas, B. Bagchi, Isomerization dynamics in viscous liquids: Microscopic investigation of the coupling and decoupling of the rate to and from solvent

viscosity and dependence on the intermolecular potential, J. Chem. Phys. 110 (1999) 7365-7375.
[49] T. Yamaguchi, N. Yoshida, K. Nishiyama, Relation between Anharmonicity of Free-Energy Profile and Spectroscopy in Solvation Dynamics: Differences in Spectral Broadening and Peak Shift in Transient Hole-Burning Spectroscopy Studied by Equilibrium Molecular Dynamics Simulation, J. Phys. Chem. B 123 (2019) 7036-7042.